128

(NASA-CR-137892) THE 100 MICRON DETECTOR DEVELOPMENT PROGRAM (Cornell Univ., Ithaca, N. Y.) 50 p HC A03/MF A01 CSCL 20F

N78-19928

Unclas

G3/74 15128

CORNELL UNIVERSITY

Center for Radiophysics and Space Research

ITHACA, N. Y.

CRSR 642

100 MICRON DETECTOR DEVELOPMENT PROGRAM

W. J. Moore

CR#137892

100 MICRON DETECTOR DEVELOPMENT PROGRAM

By W. J. Moore*

March 1976

Prepared under Contract No. NAS2-8706
J. R. Houck, Principal Investigator
Center for Radiophysics & Space Research
CORNELL UNIVERSITY
Ithaca, New York
14853

for

AMES RESEARCH CENTER

NATIONAL AERONAUTICS AND SPACE ADMINISTRATION

*On sabbatical leave from the Naval Research Laboratory, Washington, D.C. 20375.

CR#137892

FINAL REPORT

NASA Contract No. NAS 2-8706 (Cornell University)

"100 Micron Detector Development Program"

W. J. Moore*

I. INTRODUCTION

Two competing technologies exist for sensitive detection of far infrared radiation in the 100μm region: extrinsic germanium photoconductors[1] and cryogenic bolometers[2]. Both were initially developed in the early 1960's but have followed different courses of development. Germanium photoconductors are capable of submicrosecond response times and high sensitivity. They have been used primarily as detectors for submillimeter lasers and in laser spectroscopy, and secondarily in infrared astronomy. Bolometers have slow characteristic response times, especially in their highest sensitivity configuration. They have been used with grating and interferometric spectrometers where uniform spectral response is desired and in infrared astronomy.

As a result of the emphasis placed on laser spectroscopy with germanium photoconductors there has been little development of these devices for low background operation. The only previous serious development for low background use has been that of Feldman et al.[3]. In this work a minimum NEP of 1×10^{-14} watts $Hz^{-1/2}$ at 100 microns was achieved with a device operating at a temperature near $4.2^{o}K$. This result, however, is equal to the best published

*On sabbatical leave from the Naval Research Laboratory, Washington, D.C. 20375.

optical measurements for germanium bolometers although the bolometer has received far more development effort and its operating temperature is much lower.

With these considerations in mind a new effort to optimize gallium-doped germanium photoconductors (Ge:Ga) for use in space appeared appropriate and has been undertaken with the aid of this contract and a year of sabbatical study provided the author by the Naval Research Laboratory. This year of sabbatical study overlapped with a part of a similar effort conducted at Cornell University by Klaus Grossmann (Physikalisches Institut, Nussallee 12, 53 Bonn 1, Fed. Rep. Germany) in preparation for high altitude rocket studies of the upper atmosphere. The two efforts were complementary since the rocket program used detector raw material from a commercial supplier of germanium, whereas the author's program concentrated on material specially grown at the Naval Research Laboratory several years ago as part of our initial detector research program.

A large part of both programs was devoted to developing cryogenic apparatus capable of calibrating detectors under low background conditions. Some selection of amplifying circuitry and transistors was also necessary although the particular transistor used need not limit detector performance. Experimental details will be given in Section IV.

The best results obtained during the period of this contract were: for commerically produced material

$NEP_\lambda(100,150,1) = 7 \times 10^{-15}$ watts $Hz^{-1/2}$; for material grown at NRL and optimistic signal radiation calculations NEP_λ $(100,160,1) = 1.8 \times 10^{-15}$ watts $Hz^{-1/2}$. The numbers given in parentheses are the wavelength in microns, the chopping frequency in Hz, and the noise bandwidth in Hz, respectively. These results are not directly comparable since the radiation incident on the detector, the detector temperature, the method of calculating signal power, and the quantum efficiency differ in the two cases. Detailed calculations of the results with the NRL detector indicate that the device is thermal generation-recombination (g-r) noise limited with a quantum efficiency between 0.56 and 1.0 at 100 microns. The commercial material may also be g-r noise limited since its resistance was a factor of about 20 lower than that of the NRL material indicating a factor of 20 increase in carrier generation rate. A factor of 4.5 increase in NEP is expected for this situation. The results achieved indicate that the detectors are well-behaved and have quiet electrical contacts. Therefore extrapolation of these results to smaller detectors and lower detector operation temperature can be made with confidence that calculated performance can be realized.

In the course of this program, a previously observed exponential dependence of carrier lifetime on bias electric field was confirmed. An earlier measurement of resistance versus bias had suggested such a dependence but at that time it was not possible to eliminate detector heating as a possible cause of the strong resistance-bias dependence. Measurements under this program as a function of infrared background have eliminated this possibility. This increase in carrier lifetime with bias makes operation at high bias fields desirable and, in turn, requires that optimum electrical contacts be used.

Results reported here show that Ge:Ga operating near 4.2°K is, at present, at least a factor of three more sensitive than the best optical measurements published for germanium bolometers for use at 100 microns.[2] Future improvements can be achieved with smaller detectors if high quality electrical contacts are used. NEP's better than 1 x 10^{-16} watts $Hz^{-1/2}$ should be achievable.

II. SHALLOW IMPURITIES IN GERMANIUM

Impurities from groups III or V of the periodic table create shallow bound states in germanium; typical binding energies of these states are about 10 meV. Photons with energies equal to or exceeding the binding energy can free carriers from these impurities leaving an ionized impurity atom and a mobile carrier in either the conduction band (when the impurity is from group V) or the valence band (when the impurity is from group III). Any of these impurities can be used to make photo-conductive detectors. The choice of impurity to be used is based primarily on the ease with which the impurity can be introduced into germanium without simultaneously adding other undesired impurities. Undesired impurities of the type opposite that of the desired impurities (that is, acceptors in n-type material and donors in p-type material) are called compensating impurities and produce recombination centers which reduce the carrier lifetime. Of all the impurities in groups III and V, the most easily introduced in a relatively uncontaminated and controlled way is gallium. Procedures for producing high quality Ge:Ga have been described by Swiggard and Shenker[4].

Very long wavelength photoconductive detectors differ from those used at shorter wavelengths (e.g. Ge:Hg, Si:As) in that the electric field at which impact ionization of neutral impurities occurs can be quite low. Breakdown fields as low as 3.0 volts/cm have been observed in Ge:Ga. This low breakdown field has two principal causes: the ionization energy is lower than is the case for other widely used detectors (a factor of 10 lower than Ge:Hg) and the ionization energy lies below the optical phonon energy; carriers can reach energies capable of producing impact ionization before the strong optical phonon scattering can take place. Impact ionization and its attendant noise produce an upper limit on the electric field which can be used with these detectors. This, in turn, causes the photoconductive gain to be limited to values often much smaller than 1/2. This results in a somewhat lower responsivity than is the case with typical photoconductive detectors operating at shorter wavelengths. Since the responsivity is relatively low, it is necessary to be particularly careful in minimizing the noise.

Carriers in shallow impurities have large ground state radii and, therefore, these impurities cannot be introduced to high concentrations without overlap of impurity ground states. As impurity ground states begin to overlap the "hopping" and "impurity banding" processes begin to shunt the normal free carrier conduction process. This hopping conductivity is of no serious concern, however, since experimental evidence indicates that the $\eta\mu\tau$ product is optimum for impurity concentrations of the order of 1 to 2 x 10^{14} cm^{-3}, a concentration well below the onset of hopping conduction. This optimum concentration was determined for Ge:Ga using both commercially available material and material grown at NRL. Optimization was carried out with no consideration for reducing the sensitivity to nuclear or cosmic radiation. When such radiation is of concern the optimum impurity concentration may be larger than the values given here.

A widely used contacting method is either growing or ion implanting a heavily-doped region using boron impurities. Such contacts can have undesirable high-resistance regions if they are constructed using techniques which allow a gradual transition from a lightly-doped sensitive region to a heavily-doped contact region. -- As shown in Fig. 1, the sample resistance (with background infrared radiation) has a maximum at a concentration of about 1 x 10^{15} cm^{-3}. Whenever the contacting procedure produces a graded contact region in which the impurity concentration varies from less than

1×10^{15} to greater than 1×10^{15} cm^{-3}, the resistance will reach a maximum if the optical generation rate exceeds the thermal generation rate. This latter condition could occur in space missions if the device is pointed near the horizon or any other strong source. When these conditions apply, the bias electric field will fall across the high resistivity region and excess noise may be observed. A good contacting procedure should ensure that the contact is abrupt in order to minimize the likelihood of anomalous noise behavior when viewing strong sources.

Responsivity to optical (infrared) generation is maximized at an impurity concentration considerably lower than that used for detectors in the 8-14 micron window. The difference in optimum impurity concentration is understandable when the optical cross section per impurity atom for the deep and shallow impurities is compared. As an indication of the differences in optical cross section, the absorption coefficient per impurity at the ionization energy is tabulated in Table 1 for some selected impurities in germanium.

TABLE 1

Impurity	GAP	Abs. Coef/Impurity/cm^3
Ge:Ga	10.97 meV	1.05×10^{-14} cm^2
Ge:Tl	13.10 meV	7.3×10^{-15} cm^2
Ge:Be	24.45 meV	6.8×10^{-15} cm^2
Ge:Hg	91.30 meV	1.0×10^{-16} cm^2

As a result of the strong variation in absorption coefficient per impurity, the total absorption coefficient of Ge:Ga with 1 x 10^{14} impurities/cm^3 is the same as that for Ge:Hg with 1 x 10^{16} impurities/cm^3. Therefore Ge:Ga is analogous to Si:As in that large total absorption coefficients are possible by using large impurity concentrations.

Equations for the minimum detectable signal to be presented in Section III will show that only the signal-to-Johnson noise and signal-to-amplifier noise ratios are functions of $\mu\tau$. Since impurity banding occurs only after the impurity concentration exceeds about 1 x 10^{15} cm^{-3}, it is possible to construct detectors with absorption coefficients at least as high as 10 cm^{-1}. However, such detectors would have low μ-τ products and achieving the generation-recombination noise limited condition may be difficult. It is expected that Ge:Ga can be optimized for radiation environments by optimizing the impurity concentration in the same way as Si:As is optimized.

III. ELECTRICAL OPERATING CONDITIONS

Infrared detectors must be operated with biasing and amplifying circuitry appropriate to the type of detector and operating conditions expected. In this report we will consider two distinctly different operating conditions: (1) low infrared background typical of the night sky above the earth's atmosphere; the infrared flux inband (say 40-120 microns) is so small that phonon carrier generation will be the dominant generation mechanism. This is certainly appropriate for a detector operating at $4.2^{o}K$. As the bath temperature is reduced, however, other generation processes may become important. (2) Intermediate backgrounds typical of aircraft or balloon borne systems with backgrounds of the order of 1×10^{-7} watts. In this case the dominant carrier generation mechanism is optical generation and the detector resistance is lowered as a result of the higher carrier concentration.

A generally applicable set of equations for achievable NEP has been derived in a form designed to allow quick optimization of detector operating conditions. These equations differ slightly from the usual equations for detector NEP in two respects: (1) The detector is assumed to be placed in an integrating cavity or behind an aperture which defines the total amount of power available to the detector. The detector dimensions therefore do not determine the amount of power incident. A similar situation is realized for systems which are constrained to have the detector size equal to the diameter of the Airy disk. If the detector dimensions are changed, then the optical system is changed so that substantially all of the radiation from each resolution element is incident on the detector. These conditions are met with most optimized optical systems. (2) Both the detector and load resistance (feedback resistance when operational amplifiers are used in the transimpedance mode) are left in the equations. This has been done to make the optimum load resistance easier to calculate. Many formulations of detector sensitivity assume that the load resistance is much smaller than the detector resistance. When such formulations are used the photoconductive gain becomes an important parameter in the sensitivity equations. Photoconductive detectors capable of operating at very long wavelengths may have resistances comparable to that of available resistors. If the infrared background is not negligible and a conventional bias circuit is used, it is possible to maximize the signal by maximizing the load resistance. In such a case it is advantageous to use long detectors if amplifier voltage noise is the dominant noise in the system. This is just the opposite of the usual result for the small load case.

The NEP equations were derived for a uniformly illuminated detector using both a conventional load resistor and preamplifier circuit and using an operational amplifier circuit. If the first stage transistors of the two types of amplifier have the same voltage and current noise characteristics then the signal-to-noise ratio, and therefore the NEP, for the operational amplifier used in the current sensitive (transimpedance) mode and the conventional circuit are identical. The load resistance of the conventional amplifier and the feedback resistance of the operational amplifier appear in the equations for the signal-to-noise ratio in the same way. These NEP equations are, therefore, very generally applicable.

Excess 1/f noise within the detector itself cannot be expressed analytically in spite of recent advances in the understanding of this omnipresent annoyance[5,6,7]. Optimization of detectors is therefore still a black art and is likely to remain so for many years.

Separate NEP equations for each of the important noise sources (other than 1/f noise) will be given below. Since the separate noise sources are uncorrelated the overall NEP is the square root of the sum of the squares of the separate NEP's. In some situations one term can be clearly dominant and the others can be ignored. It should be noted that NEP calculations are small signal calculations. The assumption that the detector is ohmic need not be made for this situation; the NEP equations have the same form for either case. The following symbols are used in the NEP equations:

S_{ot} = the thermal carrier generation rate per unit volume (carriers cm^{-3} sec^{-1}).

S_{oo} = the optical carrier generation rate per unit volume (carriers cm^{-3} sec^{-1}).

Φ_o = the photon flux per unit volume incident on the detector (photons cm^{-3} sec^{-1}).

$h\nu$ = the energy per photon = 1.99×10^{-21} joules per photon at 100 microns

η = the detector quantum efficiency

μ = the free carrier mobility (cm^2 $volt^{-1} sec^{-1}$)

τ = the free carrier lifetime (sec.)

k = Boltzmann's constant

e	= the electron charge.
E_d	= the bias electric field (volts cm^{-1}).
T	= the detector and load (or feedback) resistor temperature (assumed the same) (Kelvins).
R_o	= the detector resistance (ac resistance if non-ohmic).
R_L	= the load (or feedback) resistance.
ℓ	= the length of the detector in the current direction (cm).
w and t	= the detector width and thickness (cm).
v_n	= the preamp voltage noise (volts $Hz^{-1/2}$).
i_n	= the preamp current noise (amps $Hz^{-1/2}$).

NEP's for the various noise sources are:

For optical generation-recombination noise

$$NEP(GRO) = 2\frac{h\nu}{\eta^{1/2}} (\Phi_o \, w\ell t)^{1/2} \quad . \tag{1}$$

For thermal generation-recombination noise

$$NEP(GRT) = 2 \frac{h\nu}{\eta} (S_{ot} \, w\ell t)^{1/2} \quad . \tag{2}$$

for Johnson noise

$$NEP(JON) = \frac{(4kT)^{\frac{1}{2}}\ell}{E_d \tau e\mu} \frac{h\nu}{\eta} \left(\frac{R_o+R_L}{R_o R_L}\right)^{\frac{1}{2}} \quad . \tag{3}$$

For Amplifier noise

$$NEP(AMP) = \frac{\ell}{E_d \tau e\mu} \frac{h\nu}{\eta} \left[v_n^{\,2}\left(\frac{R_o+R_L}{R_o R_L}\right)^2 + i_n^{\,2}\right]^{1/2} . \tag{4}$$

Of course the detector dc resistance, R_{odc}, is a function of the carrier generation rate and mobility and is given by

$$R_{odc} = \frac{\ell}{(S_{oo}+S_{ot})\tau e\mu w t} \quad . \tag{5}$$

Values for the detector parameters, methods of measuring these parameters, and results for typical Ge:Ga detectors will be discussed in Sections IV and V.

In addition to the above equations for achievable NEP it is useful to have available an expression for detector responsivity in order to compare results of optical signal measurements with the expected signal based on a knowledge of the material parameters. The voltage responsivity, $\mathbb{R}_v$, is given by

$$\mathbb{R}_v = E_d \tau e\mu \frac{\eta}{\ell h\nu} \frac{R_o R_L}{R_o+R_L} = ge\frac{\eta}{h\nu} \frac{R_o R_L}{R_o+R_L} \quad . \tag{6}$$

All the above equations can be specialized for various situations of interest. This is useful when relationships between R_L and R_o are established by system or detector constraints. For instance, if detector resistances are very much higher than any forseeable load resistor then the small load (or constant voltage) case applies. In this case the photoconductive gain remains in the responsivity equation. Such is not necessarily the case with Ge:Ga and, consequently, good results can be achieved with detectors that are somewhat larger than is customary. This is not a statement that large detectors are desirable for all circumstances, but a recognition that some freedom of choice is present.

Optimization of the detector-electronics characteristics and the optical system characteristics can be done independently since the dimensions of the detector itself need not define the resolution of the system. However, if apertures are used in front of the detector it is important that provision be made to ensure uniform detector illumination. Non-uniform illumniation can have two adverse effects: (1) Signal output is reduced if a large series resistance appears in unilluminated regions. (2) The maximum bias electric field is reduced, and thereby the signal, if large electric fields fall across the unilluminated regions.

A comment on the relationship between generation-reccmbination noise and shot noise is appropriate to clear up some confusion which exists in some published g-r noise equations. This comment is of concern whenever the photoconductive gain, g, differs appreciably from one, in particular when $g < 1$. Shot noise and generation-recombination noise are closely related and can be written in the same form. However, g-r noise differs from simple shot noise in that it is larger by a factor of $2^{1/2}$ and is a function of the photoconductive gain:

$$I_{gr}^{2} = 4egI_{o} \quad . \tag{7}$$

where I_o is the current through the detector. If $g < \frac{1}{2}$ the g-r noise can be less than the simple shot noise in a device carrying the same current. It is important to note that the simple shot noise does not exist in a device with $g \neq 1$. In fact, the g-r noise as given by Eq. 7 above is the same as the appropriate shot noise for the device.

IV. EXPERIMENTAL PROCEDURES

Laboratory calibration of long wavelength detectors for low background conditions requires careful design of the calibration system in order that sensitivities be specified with reasonable confidence. Two calibration systems have been developed under this contract. One of these systems is useful for quick turnaround tests of detectors and amplifiers but can be used with unchopped signals only. A second, more conventional, system uses a chopped signal source but requires about a day per run. Detectors have been tested in both systems and the results are in fairly good agreement.

Quick Turnaround Dipstick Test System

In order to make quick tests of detectors and amplifiers a system was constructed based on the double walled light pipe systems widely used at NRL. This system consists of three concentric thin-walled stainless steel tubes as shown in Fig. 2. The inner tube carries a black body with a carbon resistor thermometer and heater and is kept in vacuum. The second stainless tube supports the detector mount and separates the inner vacuum from the detector atmosphere, a low pressure helium gas. The third tube serves as the outer jacket and electrical shield for the preamplifier. The entire assembly passes through the neck of a standard liquid helium storage vessel. Transfer of helium to a test dewar is not required and cooldown of the detector and electronics takes 10 minutes or less. Cooldown of the blackbody in vacuum is somewhat slower, generally requiring about two hours to fall below 70°K. Calibration of the preamplifier and evaluation of the detector contacts can be completed in about 30 minutes. Complete evaluation of the detector responsivity and noise can be carried out in about three hours. The major advantage of this system is the quick turnaround capability when some component fails during prototype development of amplifiers or when initial evaluation of many detectors is desired. The system can be warmed to room temperature, modifications made, and recooled (blackbody excepted) in a half hour or less.

A more detailed drawing of the optical baffeling layout is given in Fig. 3. All surfaces below the black body aperture are primed and painted with two or more coats of 3M Velvet black paint. Surfaces below the crystal quartz window are threaded and painted black. Unwanted reflections are kept to a minimum. Apertures and spacings have been chosen to ensure that the detector can see only the black body itself, not the cold walls of the black body holder or any accidental reflected radiation from the heater. A satisfactory vacuum seal which tolerates repeated temperature cycling was made to the quartz window using a pliable adhesive ("Goo", Walthers Specialties, Inc.).

Any calibration system with close spacing between the black body and detector must be carefully constructed to prevent errors arising from: (1) Unwanted reflection from the walls of the metal components which allow radiation to reach the detector in excess of that calculated from the AΩ product. (2) Thermal coupling between the blackbody and the detector. (3) Insufficiently black emitter surface. Thermal coupling has been eliminated in this system by keeping the black body in vacuum and the detector in an exchange gas coupled to the bath. Elimination of unwanted reflection is somewhat more difficult to achieve but is believed to be small after painting all potentially reflecting surfaces with two or more coats of 3M black paint. (1) and (3) are partially self-compensating since the same coating materials are used on all surfaces.

Dewar Mounted Chopped Black Body System

Chopped black body systems are superior calibration sources since the output signal-to-noise ratio is a direct indication of the detector sensitivity. The chopped blackbody calibration device described here was initially designed by K. Grossmann but has been slightly modified. The detector is soldered to a copper mounting post which is held in close contact with the copper bottom of a laboratory helium dewar, see Fig. 4. An integrating cavity fits over the detector mounting post. Provision is made for flooding the detector compartment with helium gas for improving the thermal coupling to the dewar bottom but this provision has not yet been used. A black body is mounted on a thin walled stainless steel tube with the usual heater and carbon resistance thermometer. The entire black body, chopper, and detector space is covered by a copper shield bolted to the dewar bottom and therefore cooled to near $4.2^{\circ}K$. Extensive baffling is possible with this system to minimize unwanted reflection. It is also possible to provide glass wool absorbing material in the detector compartment and between the baffles (out of the optical path) to further minimize stray radiation. Baffling surfaces are primed, flocked, and sprayed with several layers of black paint. A crystal quartz window cooled to near $4.2^{\circ}K$ is used to isolate the detector compartment from the vacuum space. Optical details are given in Fig. 5. Aperture areas and spacings for both systems are given in Table 2.

TABLE 2

System	$A_{det}(cm^2)$	$A_{bb}(cm^2)$	d (cm)	Geometrical $A\Omega$ (cm^2ster.)
Dipstick	3.3×10^{-2}	3.3×10^{-2}	3.6	8.6×10^{-5}*
Dewar	3.3×10^{-2}	9.4×10^{-3}	13.3	1.8×10^{-6}

*The dipstick system has an effective $A\Omega$ of $2.1 \times 10^{-4} cm^2$ster. due to extraneous reflected radiation.

Two types of preamplifier have been used during the course of this work. The device with the lowest noise is a Siliconix G-118 MOSFET connected as a source follower and operated at $4.2^{o}K$. A slightly noisier, but surprisingly good, device is the Burr-Brown 3523J operational amplifier which operates at or near room temperature. The Burr-Brown amplifier cannot be ideal since it must be located on a warm surface. However, if the capacitance between the detector lead and ground is kept to a minimum the resulting noise can be adequately small if the detector contacts are quiet at high bias.

The widely used cold source follower-warm operational amplifier system was tested in several configurations. Each configuration forced compromises on the FET operating conditions or on the detector bias in order to ensure stable operation. These compromises resulted in no improvement in preamplifier noise over the more simple systems(e.g. the G-118 source follower at 20 Hz. or the Burr-Brown 3523J as transimpedance amplifier at 160 Hz.). See Fig. 6.

Comparison of noise from a Siliconix G-118 FET and that from a Burr-Brown 3523J at 20 and 160 Hz, respectively, indicates that detector noise dominates for electric fields greater than about 1.5 V/cm with the G-118 and about 2.5 V/cm with the 3523J. Of course, these bias fields will be reduced if the quality of the contacts to the sample is poor. Noise vs. bias for the two types of preamp is plotted in Fig. 7. From this plot it appears that the operational amplifier used at 160 Hz is quite adequate for bias fields of 2.5 V/cm or greater. Signal measurements indicate that the 3523J is beginning to saturate at the highest bias field so the absolute value of the noise at the detector is corrected for saturation and is accurately given in Fig. 7. A discussion of this correction will be given in the results of Section V.

Calculation of Effective Black Body Photon Flux

The effective black body photon flux was calculated by two different methods. The more accurate technique is to take the product of the relative detector sensitivity and the black body power in a small wavelength interval and sum over all possible intervals. This, of course, requires that the spectral sensitivity be measured. This has been done on a number of detectors in varying types of integrating chambers with varying results. It is difficult to guess the shape of the spectral response curve for detector A in system B based on the measured response of detector C in system D. That approach was used to calculate the lower limit (most optimistic) value for achieved NEP. The second method, which is used to calculate the upper limit (most pessimistic) NEP value, is to use as the thruput all the black body radiation in the 50 to 130 micron region. This interval corresponds to the region between the wavelength at which the cold crystal quartz window opens and the wavelength at which the detector response falls to near zero. Results using the two methods differ by a factor of less than two.

In carrying out the more optimistic calculation the spectral response given in reference 1 has been used. It is based on measurements on a detector and integrating cavity similar to those used in the tests made under this contract. This spectral response curve was multiplied by the black body power using a programmable desk top calculator. Calculations were carried out for each 5 micron spectral interval from 30 microns to 130 microns, and at each black body temperature used in the experiments. The results reported in Section V indicate that either method can give good agreement with expectations based on what is known about the material characteristics.

Electrical Contacts to Detectors

As pointed out in Section II, it is desirable to use electrical contacts which provide abrupt changes in impurity concentration between the sensitive region and the contact region. This was accomplished with grown boron single crystal contact regions as discussed by Moore and Shenker[1]. Electrical contact to the heavily doped boron region was made both by soldering with In:Ga alloy and by heating pure In to 500°C for 1 hour. The second method gives more reproduceable results. These contacts appear to be nearly ideal for large samples such as those used in these tests. The growth procedures are not easily used with the smaller detectors which would be required for closely spaced arrays or if NEP's less than 1×10^{-15} watts $Hz^{-1/2}$ are required. For these conditions new contacting procedures may have to be developed.

Integrating Cavity Design

Equation 2 above gives the achievable NEP for a thermal g-r noise limited device. This condition is not commonly encountered in infrared detector research but is, in fact, a limiting factor for Ge:Ga cooled by liquid helium at 4.2°K. This will be discussed in Section V. When thermal g-r noise dominates, the NEP is proportional to $1/\eta$ and η must therefore be kept as large as possible. An integrating cavity is a simple approach to satisfying this requirement. Typical cavities used in these measurements were right circular cylinders, closed at one end by the detector mounting post and at the other by a plate with a small hole to pass the detector bias lead. A small aperture in the side of the cylinder admits a calculable amount of signal power. This aperture is smaller than the detector and would allow the detector to be non-uniformly illuminated if the cavity were not inclined 45° to the light path. This inclination also improves the efficiency of the cavity resulting in quantum efficiencies perhaps as high as 1.0.

V. RESULTS

Before presenting the results of the detector measurements it will be useful to present some measurements of material properties which are important in determining the characteristics of detectors. The detector measurements will then be presented and will be shown to be consistent with the material characteristics. Material characteristics of primary importance are free carrier lifetime, breakdown electric field, carrier mobility, and thermal carrier generation rate. These characteristics determine the responsivity, thermal generation-recombination noise, and Johnson noise.

Free carrier lifetimes have been measured by Moore and Shenker[1] for Ge:Ga of the same quality as that used in these tests. These results have been replotted on semi-logarithmic paper to show that the lifetime is an exponential function of bias electric field over the range of interest for detector operation. This data is given in Fig. 8. Also shown on this figure is a measurement, using the Hall effect, of carrier concentration as a function of bias field on material from the same ingot. It is clear that the carrier concentration is changing with the carrier lifetime as expected. Lifetimes could not be measured for values of τ less than about 1×10^{-7} sec so τ values less than that value were determined by extrapolation using the Hall effect and sample conductivity measurements.

The resistivity vs. electric field of several detectors with varying background infrared illumination has been determined. Some of this data is plotted in Fig. 9. All curves fit a relationship of the form

$$\rho = \rho_o e^{-\alpha E} \qquad (8)$$

with α values ranging from 0.89 to 1.36 cm volt^{-1}. Slight changes in α due to varying the background photon flux have been ovserved but the greatest changes occur after the heat treatment used to improve the indium-to-boron-doped germanium contact region. All samples which have heat treated contacts have α values less than 1 whereas the two samples measured without heat treatment have α values greater than 1. One sample measured using a 4-point technique and simple soldered contacts also has α slightly less than 1. It can be concluded that a small decrease in contact resistance with increasing bias is responsible for the larger α values measured on samples without heat-treated contacts. Some error in α also occurs due to uncertainty in the measurement of detector length. The grown boron-doped germanium regions cannot be made in a way that provides contact regions precisely perpendicular to the current path. Each detector's length, therefore, varies across its width. This error is of the order of ± 5% and results in a ± 5% error in α. The observed values of α are summarized in Table 3.

TABLE 3

Sample	α (cm/volt)	Background photon flux (photons/sec.)	History
Ge:Ga 412 D	0.89	$\sim 2.4 \times 10^{18}$	Contacts annealed 500°C, 1 Hr.
Ge:Ga 412 D	0.95	$\sim 4.6 \times 10^{16}$	Contacts annealed 500°C, 1 Hr.
Ge:Ga 412 D	0.95		4-point I-V meas.
Ge:Ga 412 -	1.36	$\ll 1 \times 10^{12}$	New contacts, not annealed
Ge:Ga 7-56BF-1	1.07	$\ll 1 \times 10^{12}$	New contacts, not annealed
Ge:Ga 7-56BF-2	0.91	$\ll 1 \times 10^{12}$	Contacts annealed 500°C, 1 Hr.

If the large α values are attributed to contact effects, as discussed above, the true value must be of the order of 0.95. That is, the lifetime varies as

$$\tau(E) = \tau(o)\, e^{0.95E} \qquad (9)$$

in the bias region above 1 V/cm.

The exponential dependence of conductance on bias is seen in the dipstick detector measurements of conductance as a function of black body emission. A typical dipstick run is reproduced in Fig. 10. Since the dipstick had tighter physical dimensions than the dewar system it was more susceptible to stray reflected radiation above that calculated from the geometrical etendue. Fig. 10 has been corrected for this effect by requiring the change in conductance per watt of incident power to agree with that measured in the more precise dewar system. The effective etendue for the dipstick system which is required to give agreement is 2.1 x 10^{-4} cm^2ster. As a check on the effect of direct heating of the detector a run was made with glass wool absorbing material above the sample. The results of this check are also shown in Fig. 10. It is clear that direct heating is negligible.

Noise data has already been presented for the dipstick system using a G-118 FET source follower in Fig. 7. The conductance versus black body power data and the noise data allow an approximate NEP to be determined. This NEP is plotted in Fig. 11. Since this data was taken at 20 Hz and is for a detector without annealed contacts, it does not represent optimum results. It does, however, give an indication of the kind of results achievable with the quick turn-around dipstick system. Improvements in the dipstick system are possible so it is not necessarily a limit to the system performance capabilities.

A particularly useful technique for determining the compensation ratio and the carrier concentration at the operating condition is the temperature dependence of the Hall effect. Such data was taken several years ago on sample Ge:Ga 412- and is reproduced here in Figs. 12(a) and 12(b). Light leaks in the system prevented reduction of the carrier concentration below about 1×10^4 cm^{-3} and distort the curve near 4.2^oK. However, the activation energy determined from this curve is quite accurate so the linear part can be extrapolated to determine the carrier concentration for an ideally dark system. Extrapolation to temperatures lower than 4.2^oK can be made with good accuracy but should be qualified with the caution that the point at which impurity banding or hopping conductivity begins to contribute significant conductivity is unknown.

With these dc results as background we can now continue to a discussion of measurements made in the chopped black body system. Detector dc conductance and signal at 160 Hz are plotted in Fig. 13 as a function of bias electric field. The dc conductance increases for all fields whereas the ac signal saturates at the largest bias. This saturation is attributed to saturation of the Burr-Brown 3523J operational amplifier as its dc output approaches its maximum value. This point at which the dc output reaches the maximum value given by the manufacturer is indicated in Fig. 13 and is consistent with the assumption that the signal output saturates at that bias. This effect does not change the signal-to-noise ratio but does change the apparent signal output per watt of input power. The correction is shown by a dashed line running parallel to the dc data. The noise for this system has already been given in Fig. 7.

The ratio of the rms noise-per-$Hz^{1/2}$ to the rms signal per rms watt of effective black body power is the NEP. This is plotted in Fig. 14 as a function of bias. This figure is plotted for the most optimistic conditions and reaches a minimum at $NEP_\lambda = 1.8 \times 10^{-15}$ watts $Hz^{-1/2}$ for $\lambda = 100$ microns. The consistency of measurements of conductivity, signal, and noise require that the quantum efficiency, η, at $\lambda = 100$ µm be 1.0 ($\eta \approx .50$ @ 75µm) with the optimistic assumptions.

A careful analysis of the measurements of dc conductivity (assumed to be due to thermal carrier generation), ac signal and noise has been carried out. Since the dc conductance is due to thermal generation it can be written as

$$G_o = S_{ot} \tau e \mu \frac{wt}{\ell} \quad . \qquad (10)$$

This Eq. is solved for $S_{ot} wt\ell$ (the total thermal generation rate) to be used in the NEP Equation (Eq.2). Then

$$NEP(GRT) = 2 \frac{h\nu}{\eta} \left(\frac{G_o \ell^2 \eta}{\eta \tau \mu e}\right)^{1/2} \quad . \qquad (11)$$

The quantity $\eta \tau \mu e \ell^{-2}$ can be calculated from the signal if the effective signal power is known.

The voltage responsivity, $\Re_V$, is given by Eq. 6 above. Other responsivities can be defined to remove known dependences on bias potential and on load or feedback resistor. If the preamplifier is a current-sensitive operational (transimpedance) amplifier then the voltage responsivity is

$$\Re_V \equiv \frac{\langle \Delta Vsig \rangle_{rms}}{\langle \Delta Psig \rangle_{rms}} = V_d \frac{\langle \Delta Gsig \rangle_{rms}}{\langle \Delta Psig \rangle_{rms}} R_F \quad . \tag{12}$$

The current responsivity, R_I, is

$$\Re_I = \frac{\Re_V}{R_F} = V_d \frac{\langle \Delta G \rangle_{rms}}{\langle \Delta P \rangle_{rms}} \quad . \tag{13}$$

A third responsivity, to be called the conductance responsivity, denoted $\Re_G$, is defined by

$$\Re_G = \frac{\langle \Delta G \rangle_{rms}}{\langle \Delta P \rangle_{rms}} = \frac{\Re_V}{V_d R_F} \quad . \tag{14}$$

This responsivity depends on detector parameters and photon energy but not on the bias conditions except insofar as the bias conditions alter the detector parameters [e.g. $\tau(E)$]. In terms of detector parameters:

$$\Re_G = \frac{\eta \tau e \mu}{h\nu \ell^2} \quad . \tag{15}$$

Solving for $\eta \tau e \mu \ell^{-2}$ gives

$$\eta \tau e \mu \ell^{-2} = \Re_G h\nu \quad . \tag{16}$$

Then

$$NEP(GRT) = 2 \left(\frac{h\nu}{\eta}\right)^{1/2} \left(\frac{G_o}{\Re_G}\right)^{1/2} \quad . \tag{17}$$

G_o and $\Re_G$ are measured quantities and the photon energy $h\nu$ is known since the power has been expressed as effective power at the wavelength of peak response (100 μm). The only remaining unknown variable is η which is then adjusted to give agreement between the measured NEP and that calculated from Eq. 17. Adjusting the quantum efficiency forces the calculated signal and thermal g-r noise to agree with the measured signal and noise. If the resulting η does not fall within the range of reasonable values ($0.2 \leq \eta \leq 1.0$ with an integrating cavity) then the procedure for determining the effective signal power is questioned. Additionally, the measured R_G, assumed η, known ℓ and e provide a calculation of the $\tau\mu$ product. If τ is taken from Fig. 8 then μ can be calculated and compared with known values from Hall effect data on similar samples. The thermal generation rate per unit volume S_o can be determined from Eq. 10 and used to determine the detector temperature with the aid of Fig. 12(b) and the approximate impurity concentration. Results for the folded spectral response method and for the power inband method of calculating effective signal power are given for the 3.0 V/cm point and $\tau = 1.7 \times 10^{-7}$ sec in Table 4 (following page).

The prospect for future improvement is quite good. Since the limit is now due to thermal g-r noise it should be quite easy to improve performance by cooling the detector below 4.7°K or by reducing its volume. Cooling can be done with no required changes in the detector but may require amplifier improvements in order that the lower noise performance be realized. A reduction in detector size is also desirable. This is not easily done when grown boron contacts are used. New contacting techniques would be very helpful in making this approach to improvement more realistic.

TABLE 4

Characteristics of a Ge:Ga detector with dimensions 1.6 x 1.8 x 6.6mm operated at 3.0V/cm. The hole lifetime is assumed to be 1.7×10^{-7} sec.

	Folded Spectrum	Power inband
NEP (watts $Hz^{-1/2}$)	1.8×10^{-15}	3.2×10^{-15}
η (at λ = 100 μm)	1.0	0.56
$\mathfrak{R}_V$ (volts $watt^{-1}$)	5.5×10^9	3.2×10^9
$\mathfrak{R}_I$ (amps $watt^{-1}$)	3.4	2.0
$\mathfrak{R}_G$ (Ω^{-1} $watt^{-1}$)	1.9	1.1
μ (cm^2 $volt^{-1}$ sec^{-1})	6.0×10^4	6.2×10^4
g	4.6×10^{-2}	4.8×10^{-2}
S_o (cm^{-3} sec^{-1})	5.6×10^{12}	5.4×10^{12}
T (Kelvins)	~ 4.7	~ 4.7

REFERENCES

1. W. J. Moore and H. Shenker, I. R. Phys. 5, 99 (1965).

2. F. J. Low and A. R. Hoffman, Appl. Optics 2, 649 (1963). For a review of bolometer sensitivites see N. Coron, G. Dambier, and J. Lablanc in "Infrared Detection Techniques for Space Research", 5th ESLAB Symposium, V. Manno and J. Ring, Eds., ; 1972.

3. P. D. Feldman and D. P. McNutt, Appl. Optics 8, 2205 (1969).

4. E. M. Swiggard and H. Shenker, J. Electrochem. Soc. 113, 92 (1966).

5. F. N. Hooge, Phys. Lett. 29A, 139 (1969).

6. P. H. Handel, Phys. Rev. Lett. 34, 1492 (1975).

7. R. F. Voss and J. Clark, Phys. Rev. Lett. 36, 42 (1976).

FIGURE CAPTIONS

1. Resistance of boron-doped germanium samples with various impurity concentrations. All samples had the same dimensions and infrared background. The effect of bias is also shown.
2. Dipstick test system, physical construction.
3. Dipstick test system, optical baffling details.
4. Dewar test system, physical construction.
5. Dewar test system, optical baffling details.

6a. Source-follower amplifier.

6b. Transimpedance amplifier.

7. Noise of Ge:Ga detectors in the cold dark with Siliconix G-118 FET source-follower and Burr-Brown 3523J op-amp preamplifiers. $R_L(R_F) = 1.6 \times 10^9 \Omega$.
8. Carrier concentration from Hall effect and free carrier lifetime from Ref. 1.
9. Resistivity of Ge:Ga detectors. Sample Ge:Ga 412D was measured with two different infrared backgrounds. All other samples had the minimum infrared background possible in the systems used.
10. Conductance-bias characteristic of Ge:Ga in the dipstick test system for different blackbody temperatures. Identical measurements with glass wool IR absorbing material between the detector and source are also shown.

11. NEP in the dipstick system with effective dipstick AΩ and folded spectrum blackbody power.

12.(a) and (b). Hall carrier concentration.

13. Detector conductance and signal in the dewar system.

14. Detector NEP in the chopped system. The more optimistic signal power calculations have been used.

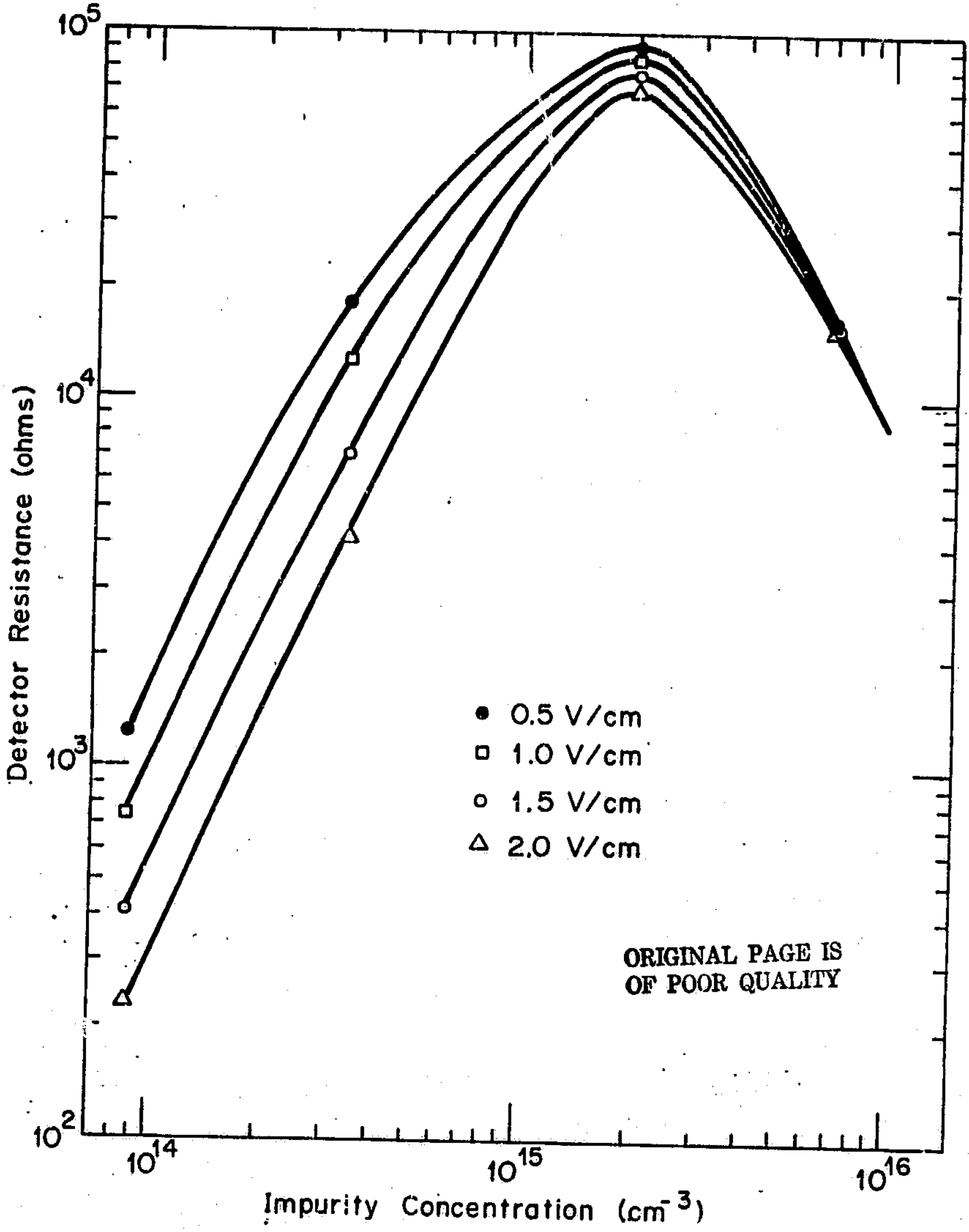

Detector Resistance (ohms)
Impurity Concentration (cm^{-3})
10^5
10^4
10^3
10^2
10^{14}
10^{15}
10^{16}
0.5 V/cm
1.0 V/cm
1.5 V/cm
2.0 V/cm

Figure 1

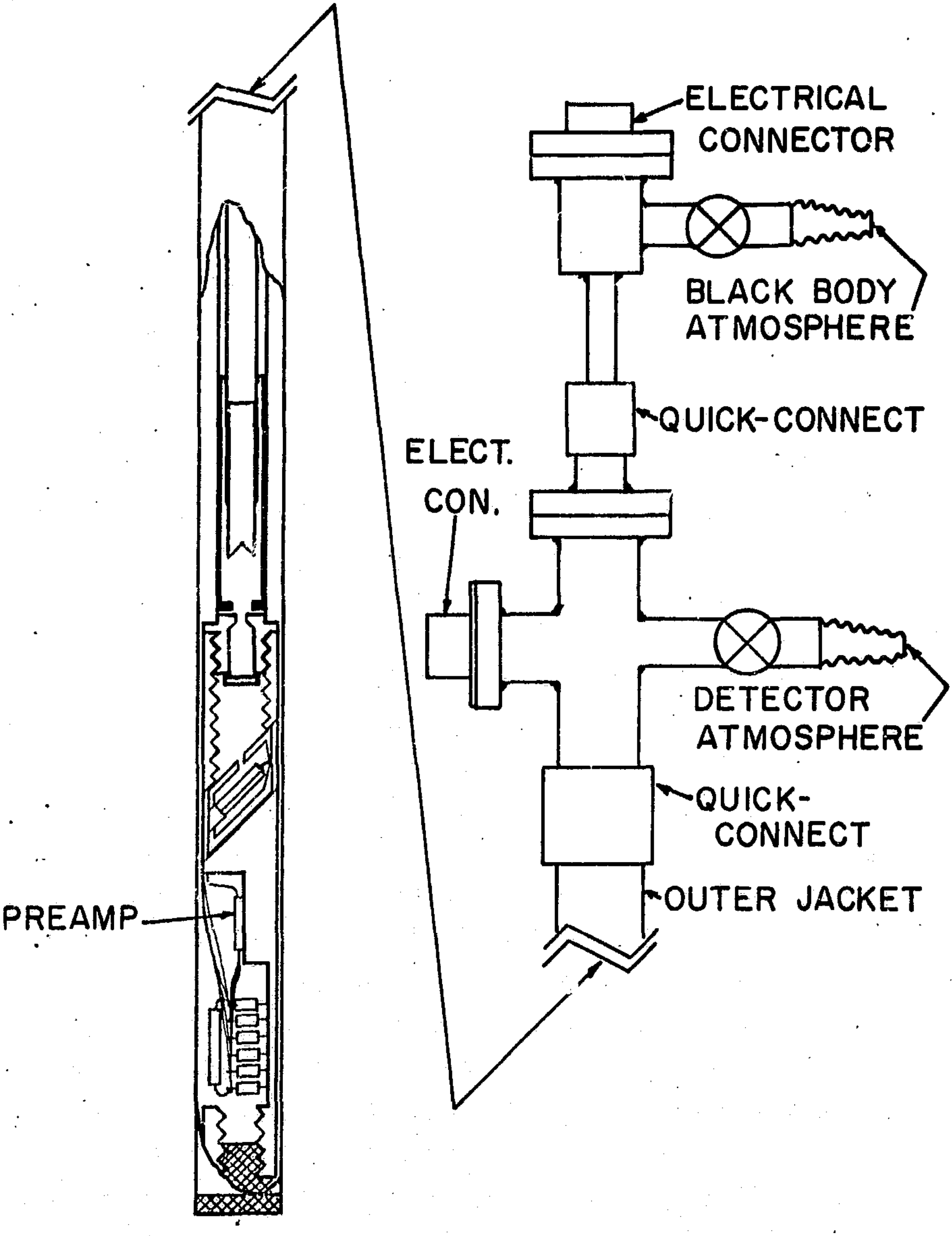

ELECTRICAL CONNECTOR
BLACK BODY ATMOSPHERE
QUICK-CONNECT
ELECT. CON.
DETECTOR ATMOSPHERE
QUICK-CONNECT
OUTER JACKET
PREAMP

Figure 2

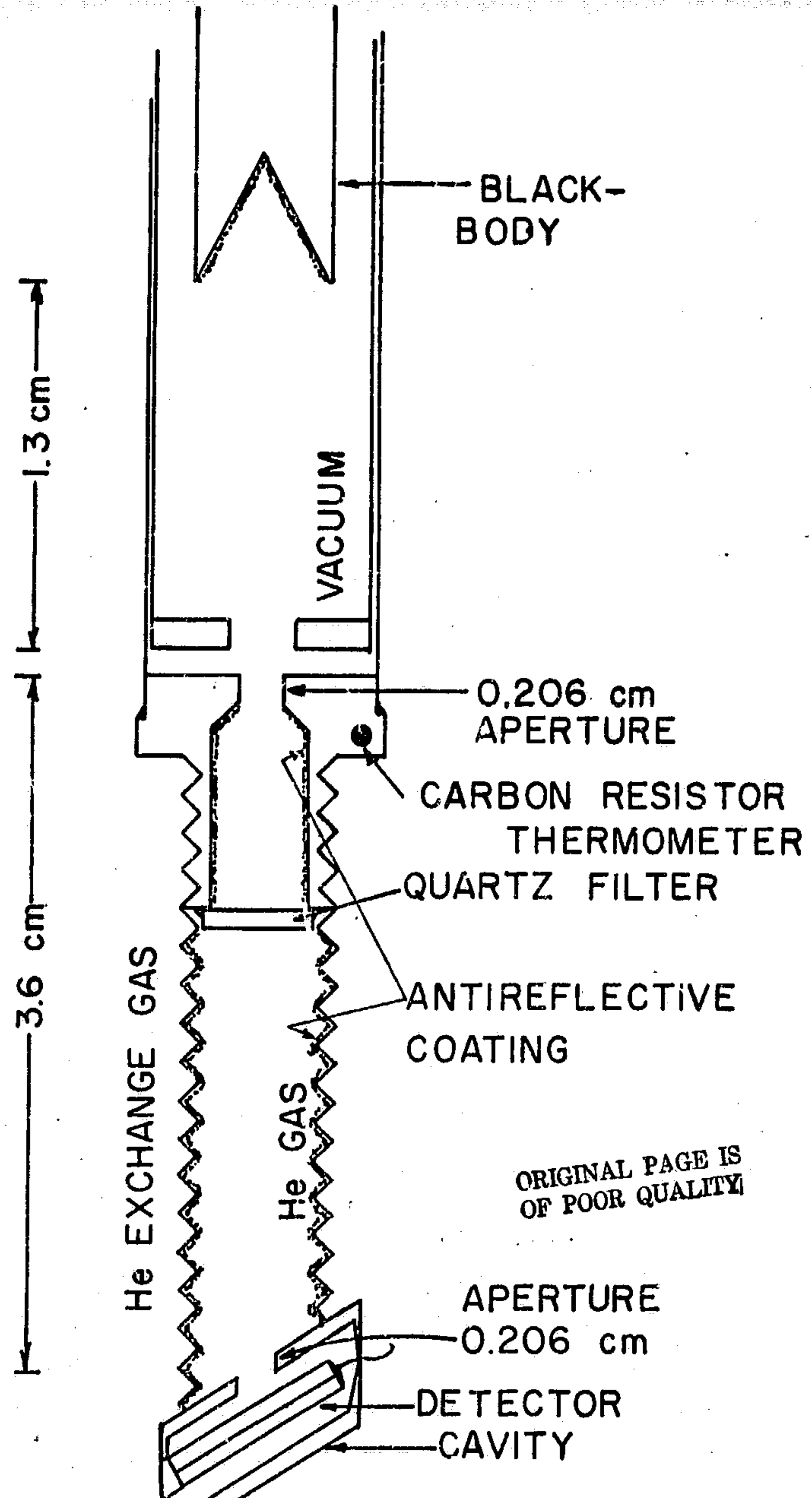
BLACK-
BODY
1.3 cm
VACUUM
0.206 cm
APERTURE
CARBON RESISTOR
THERMOMETER
QUARTZ FILTER
3.6 cm
ANTIREFLECTIVE
COATING
He EXCHANGE GAS
He GAS
APERTURE
0.206 cm
DETECTOR
CAVITY

Figure 5

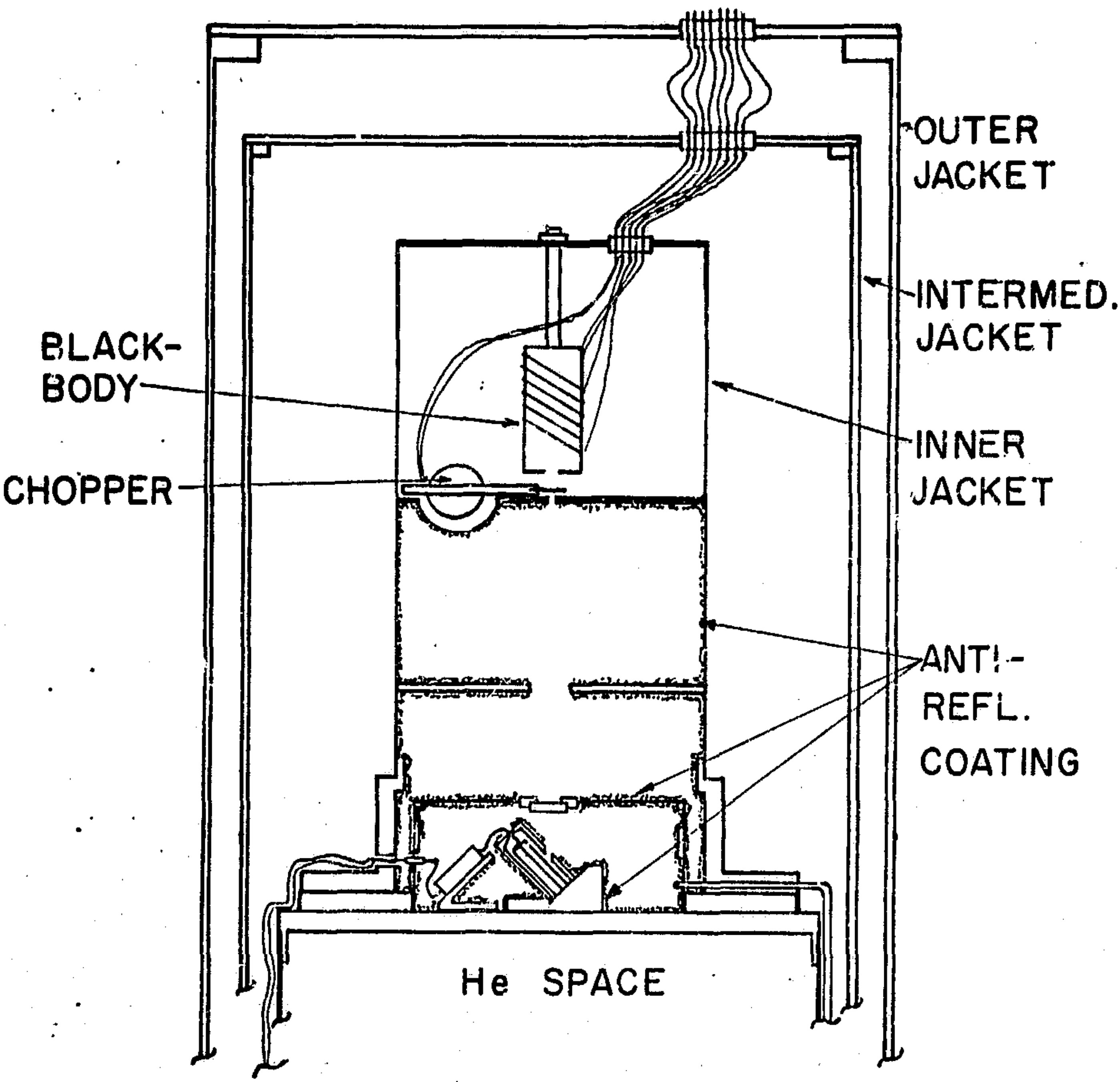
OUTER
JACKET
INTERMED.
JACKET
BLACK-
BODY
INNER
JACKET
CHOPPER
ANTI-
REFL.
COATING
He SPACE

Figure 4

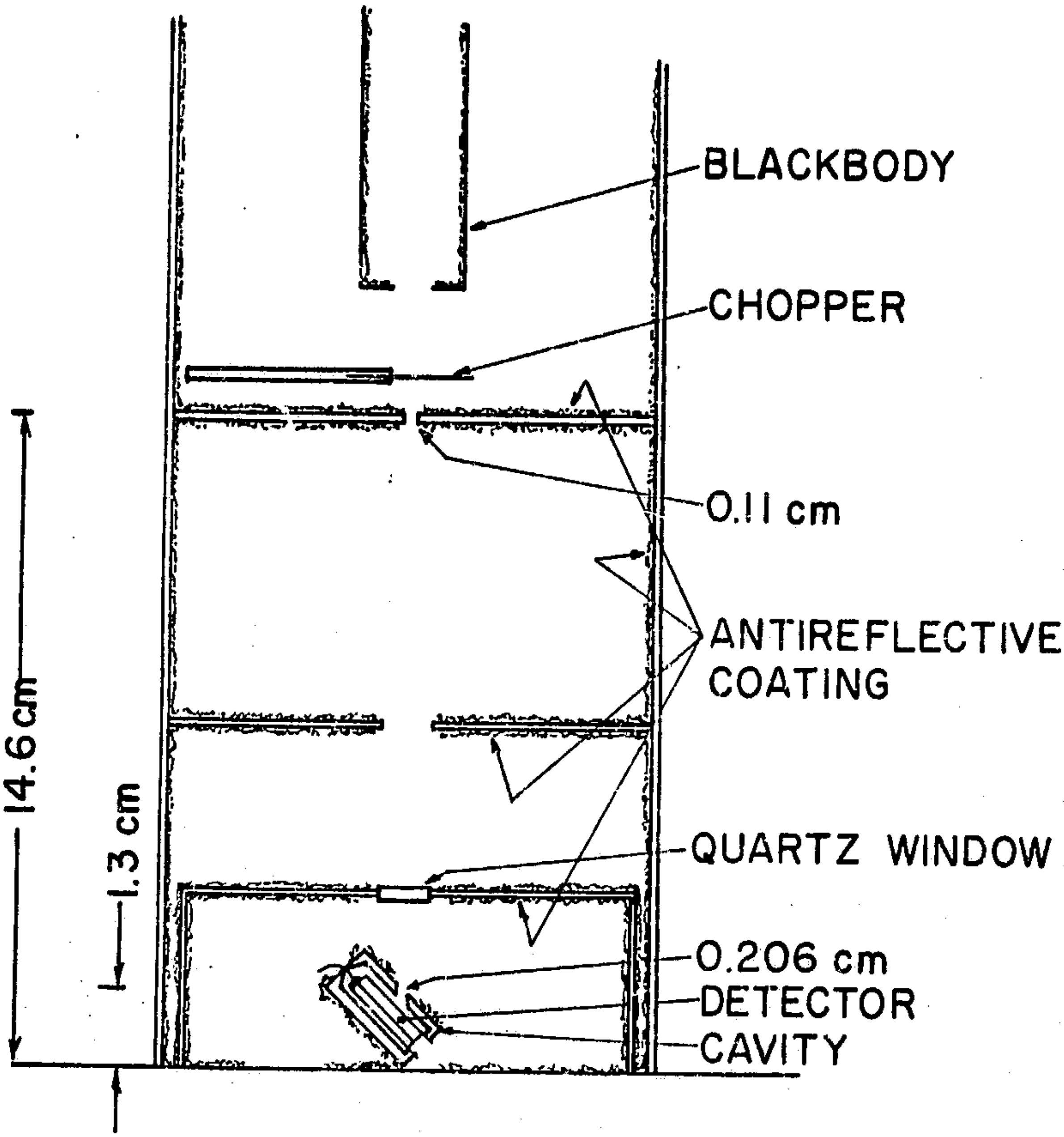

SCHEMATIC BAFFLING LAYOUT

Figure 5

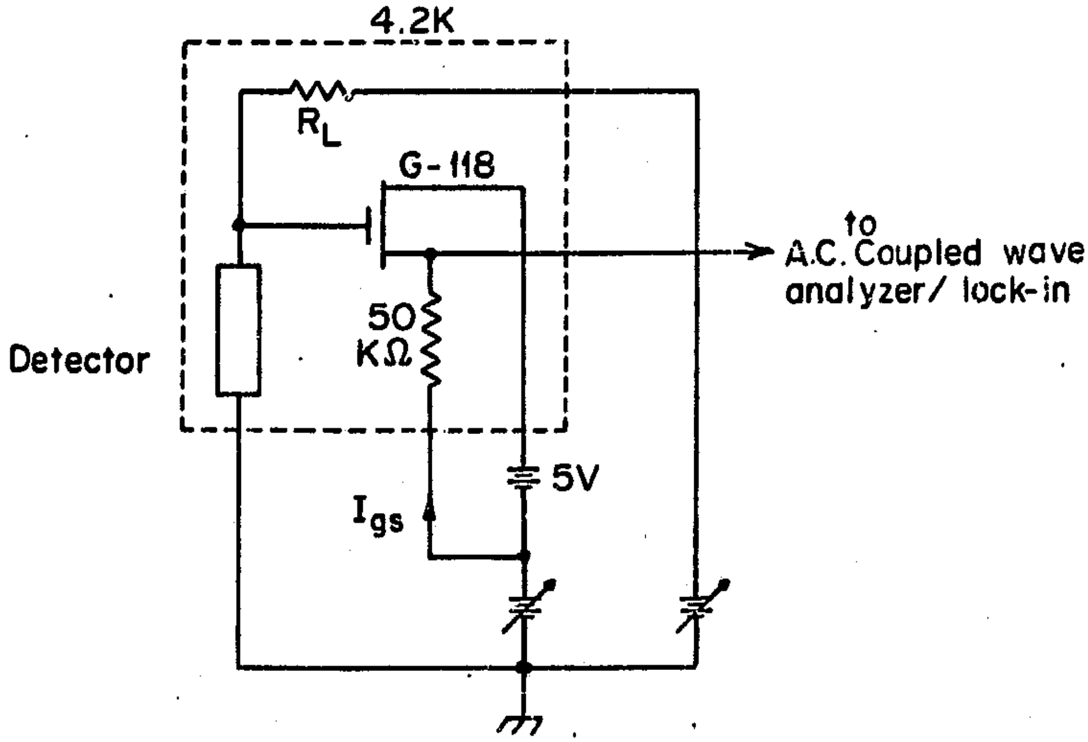
4.2K
R_L
G-118
to
A.C. Coupled wave
analyzer/ lock-in
50
KΩ
Detector
5V
I_{gs}

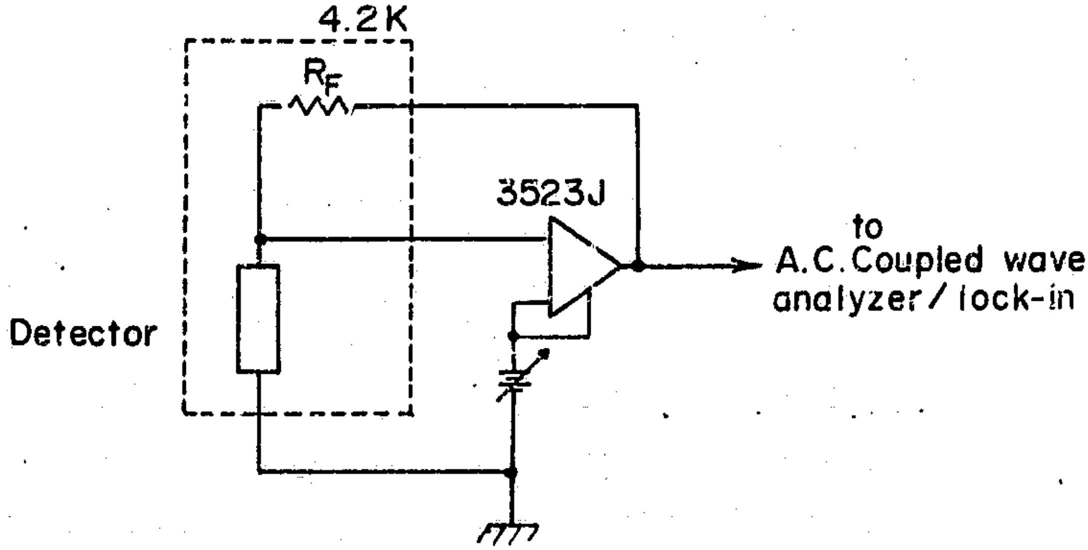
4.2K
R_F
3523J
to
A.C. Coupled wave
analyzer/ lock-in
Detector

Figure 6

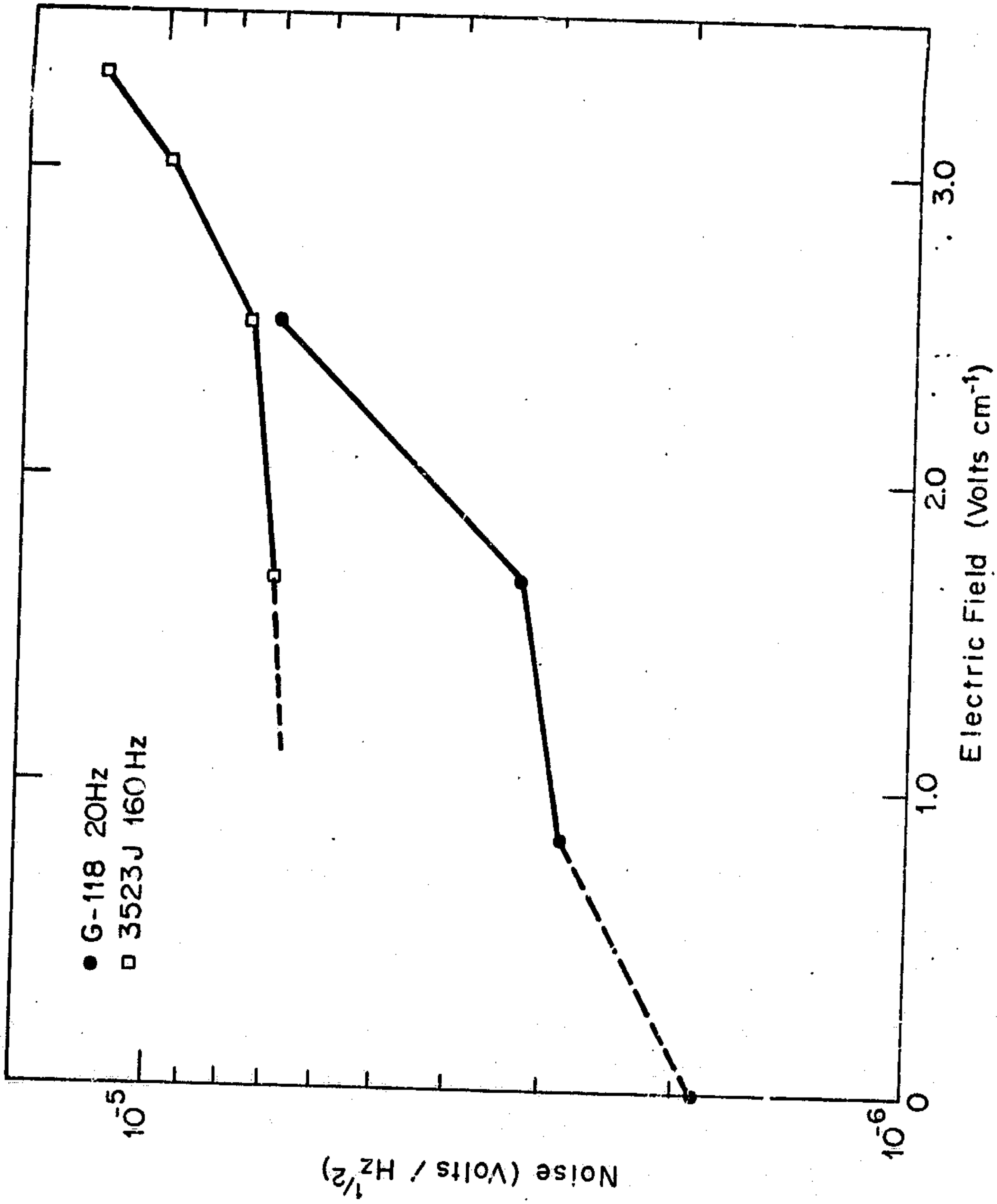

G-118 20Hz
3523J 160 Hz
Electric Field (Volts cm⁻¹)
Noise (Volts / Hz^1/2)
0
1.0
2.0
3.0
10⁻⁶
10⁻⁵

Figure 7

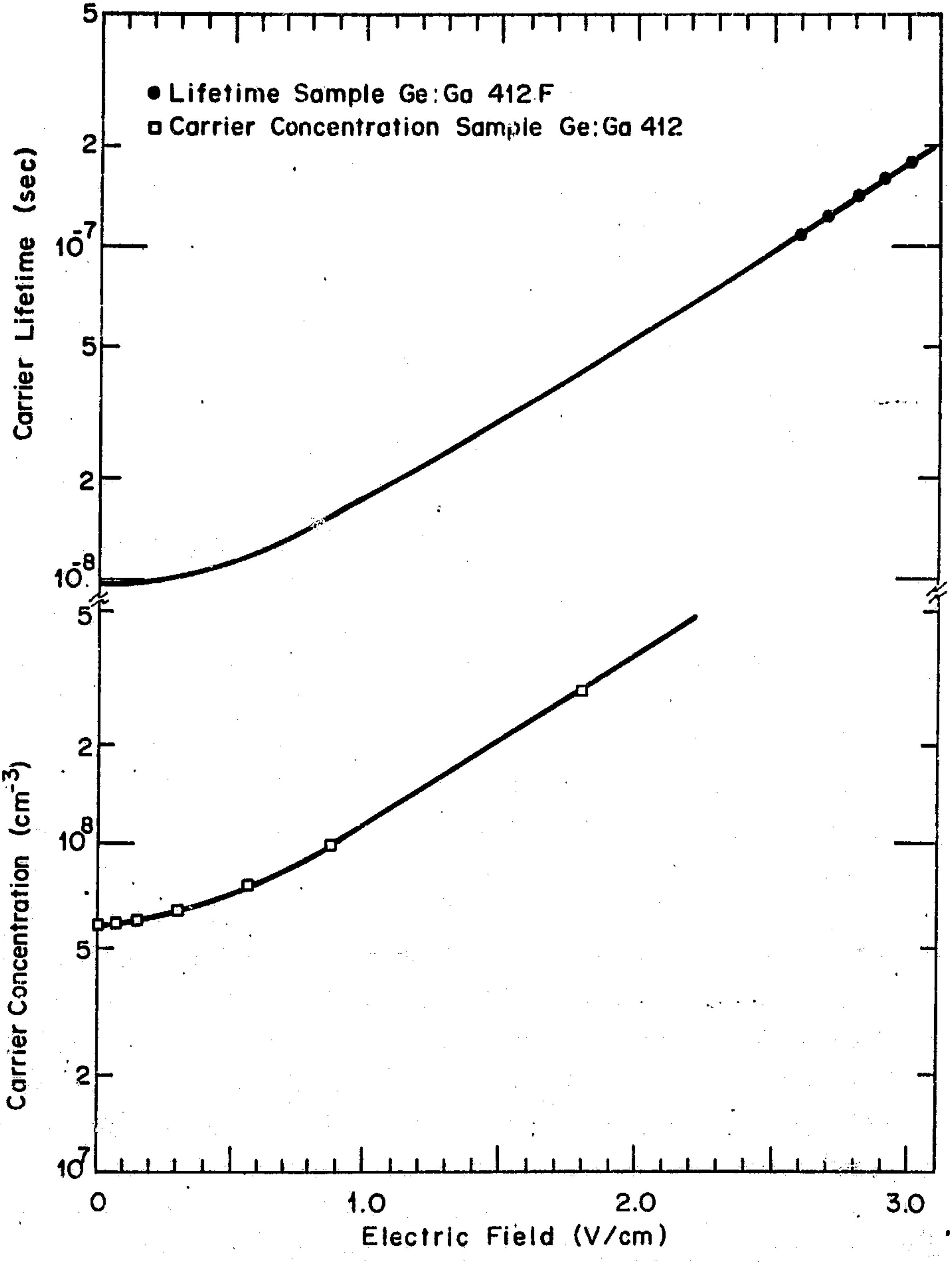

Lifetime Sample Ge:Ga 412 F
Carrier Concentration Sample Ge:Ga 412
Carrier Lifetime (sec)
Carrier Concentration (cm^{-3})
Electric Field (V/cm)
5
2
10^{-7}
5
2
10^{-8}
5
2
10^{8}
5
2
10^{7}
0
1.0
2.0
3.0

Figure 8

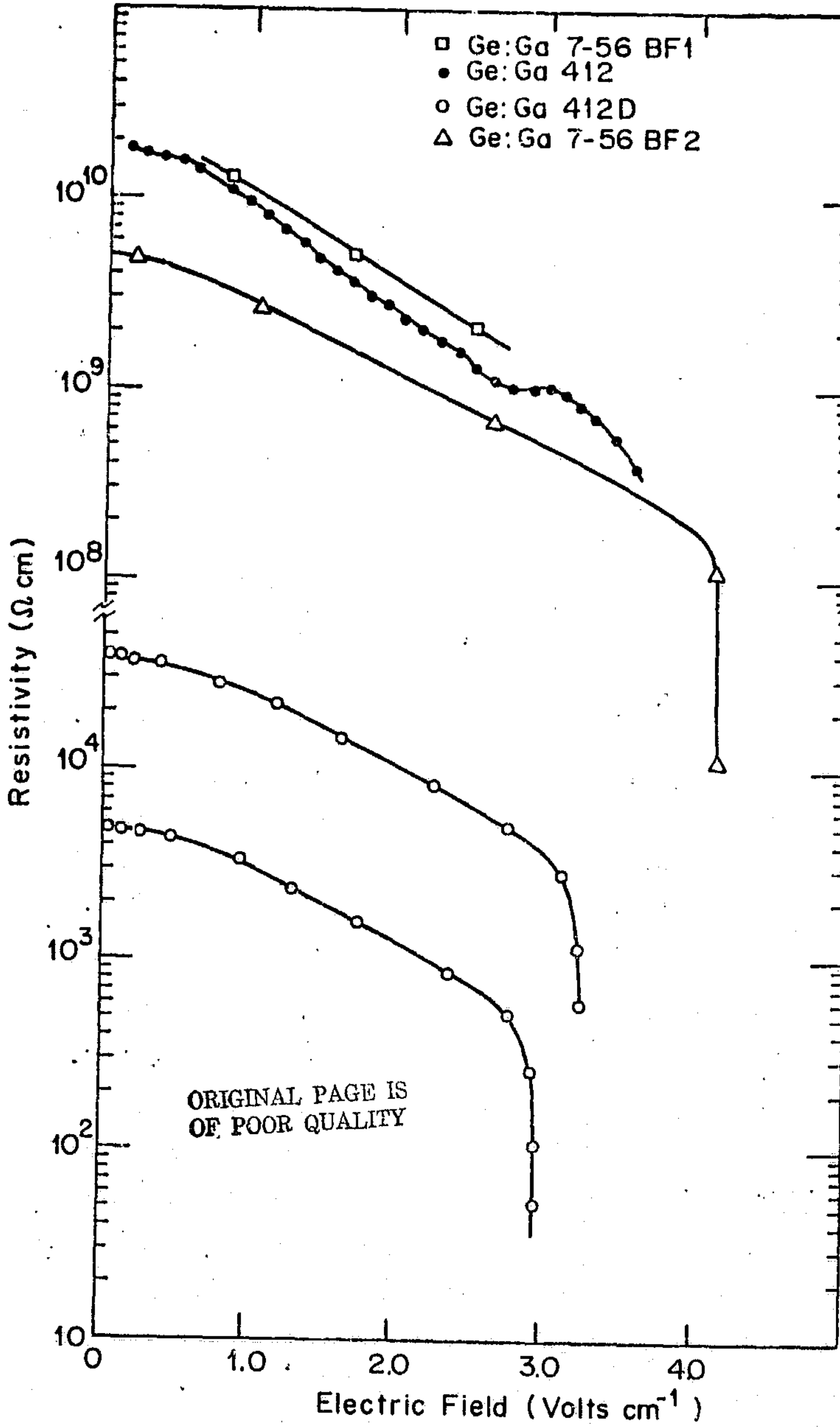

Ge:Ga 7-56 BF1
Ge:Ga 412
Ge:Ga 412D
Ge:Ga 7-56 BF2
Resistivity (Ω cm)
Electric Field (Volts cm^{-1})
10^{10}
10^{9}
10^{8}
10^{4}
10^{3}
10^{2}
10
0
1.0
2.0
3.0
4.0

Figure 9

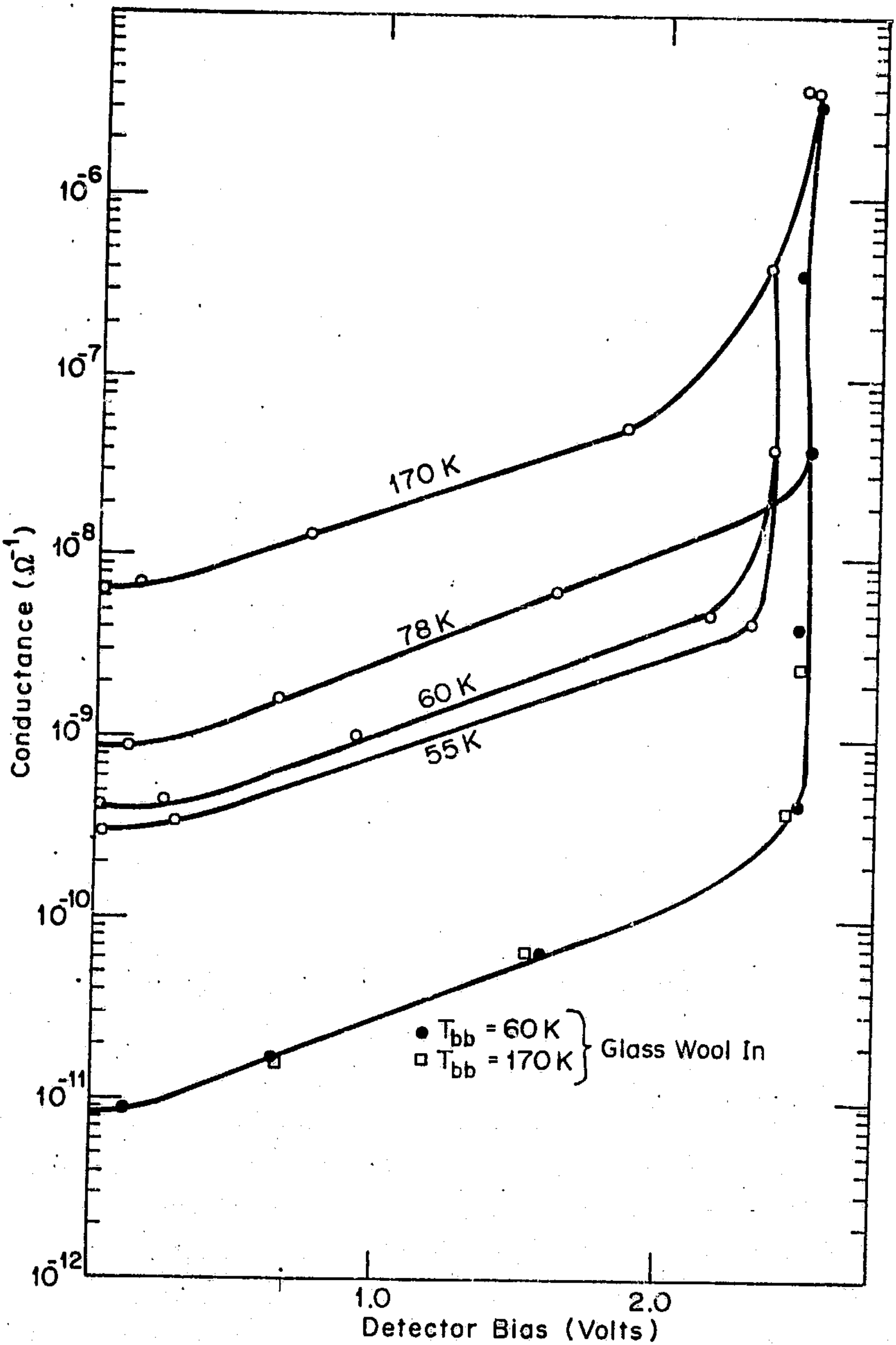

10^{-6}
10^{-7}
10^{-8}
10^{-9}
10^{-10}
10^{-11}
10^{-12}
Conductance (Ω^{-1})
170 K
78 K
60 K
55 K
● T_{bb} = 60 K
□ T_{bb} = 170 K
Glass Wool In
1.0
2.0
Detector Bias (Volts)

Figure 10

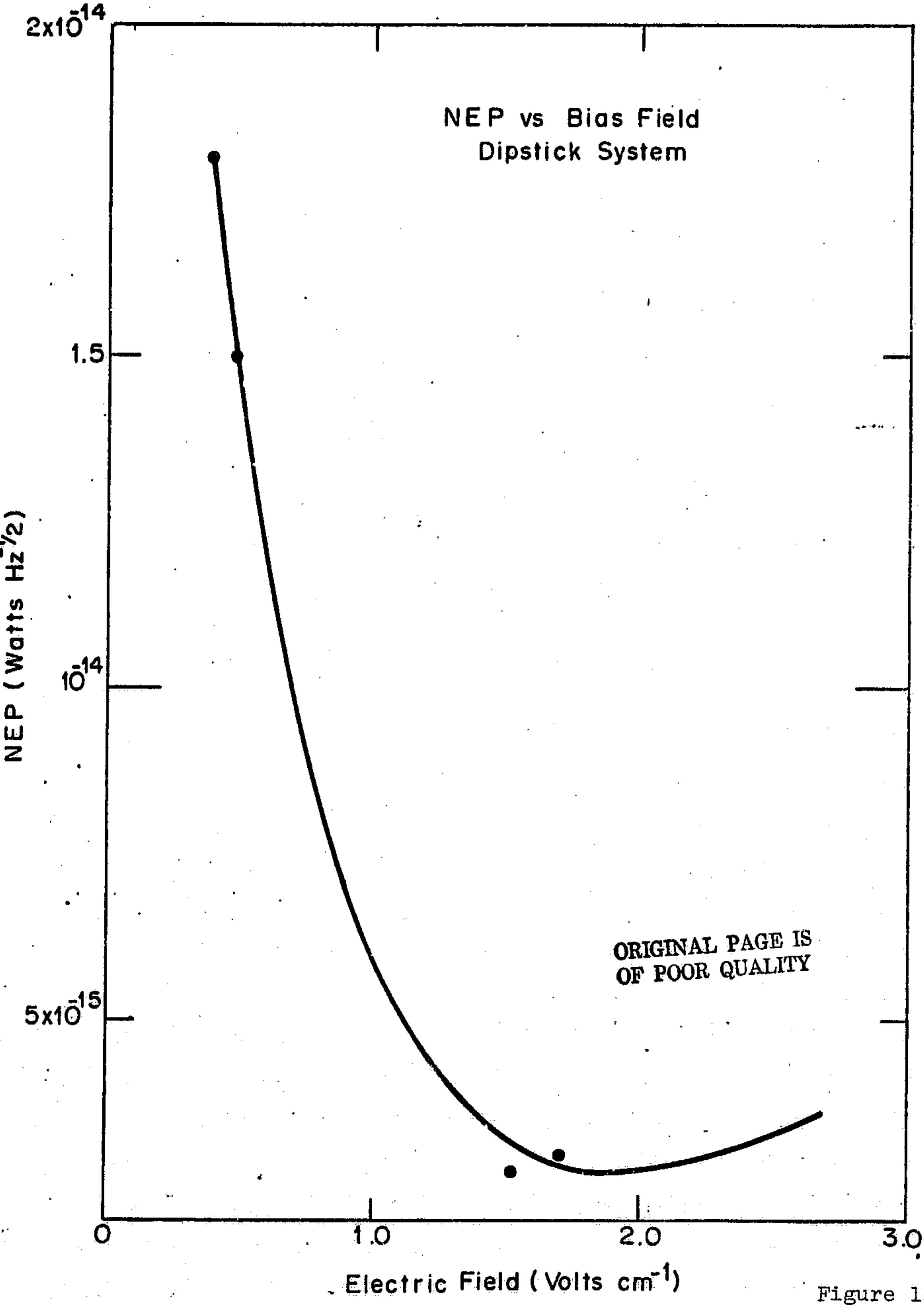

NEP vs Bias Field
Dipstick System
ORIGINAL PAGE IS
OF POOR QUALITY
2x10^-14
1.5
10^-14
5x10^-15
NEP (Watts Hz^-1/2)
0
1.0
2.0
3.0
Electric Field (Volts cm^-1)

Figure 11

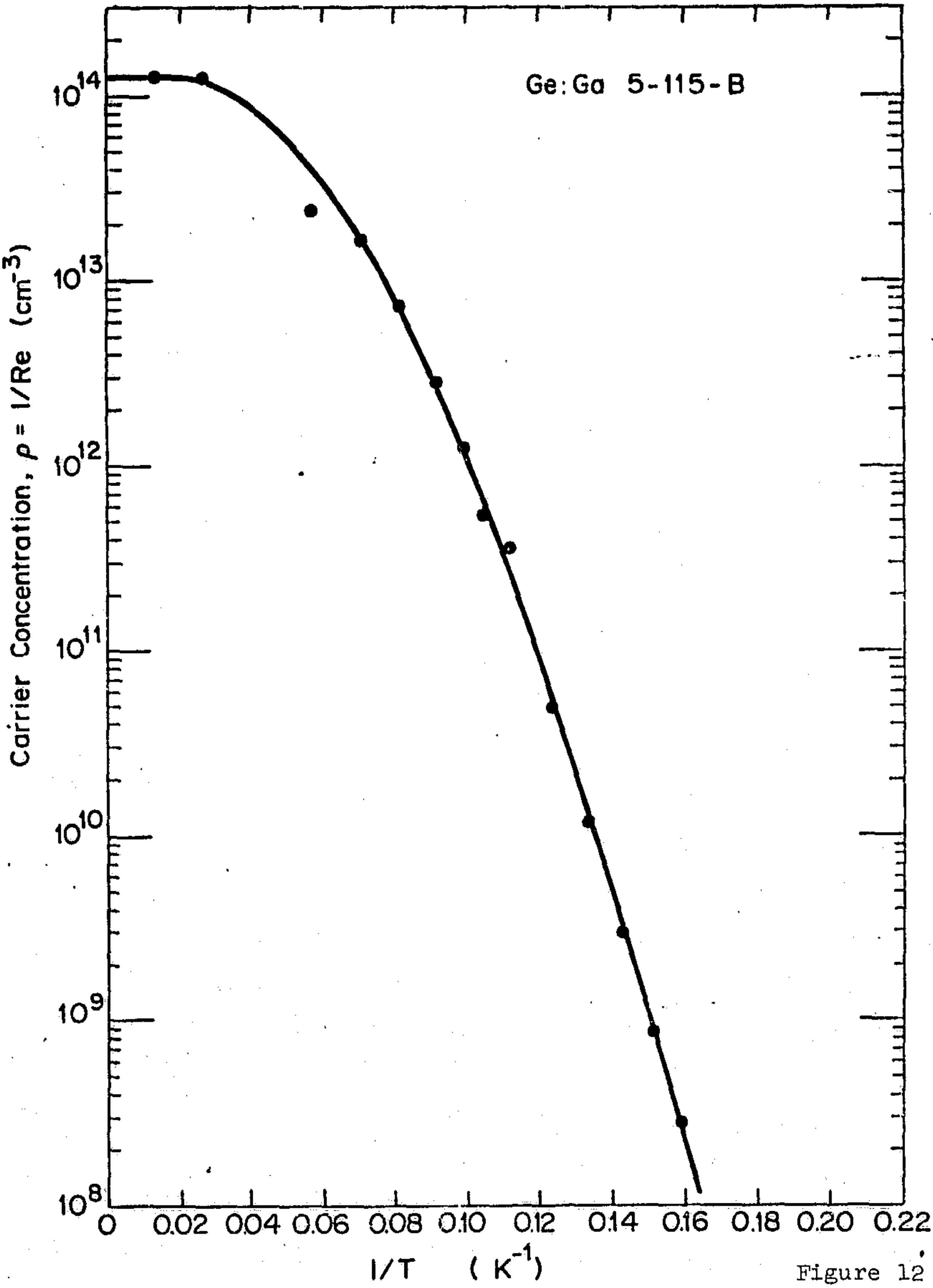

Ge:Ga 5-115-B
Carrier Concentration, ρ = 1/Re (cm⁻³)
10^14
10^13
10^12
10^11
10^10
10^9
10^8
0
0.02
0.04
0.06
0.08
0.10
0.12
0.14
0.16
0.18
0.20
0.22
1/T (K⁻¹)

Figure 12 a

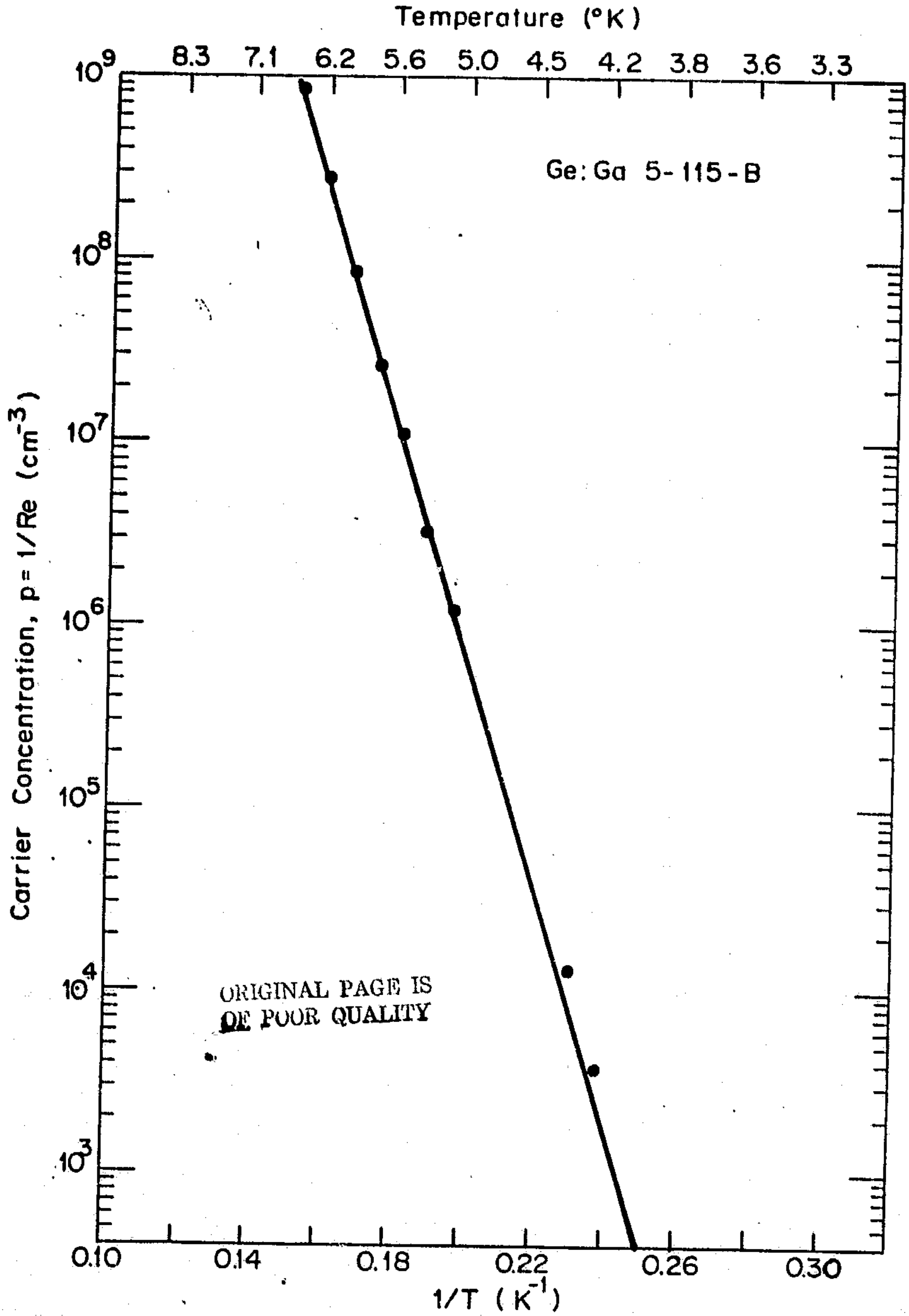
Temperature (°K)
8.3
7.1
6.2
5.6
5.0
4.5
4.2
3.8
3.6
3.3
Ge: Ga 5-115-B
Carrier Concentration, p = 1/Re (cm^{-3})
10^9
10^8
10^7
10^6
10^5
10^4
10^3
0.10
0.14
0.18
0.22
0.26
0.30
1/T (K^{-1})

Figure 12 b

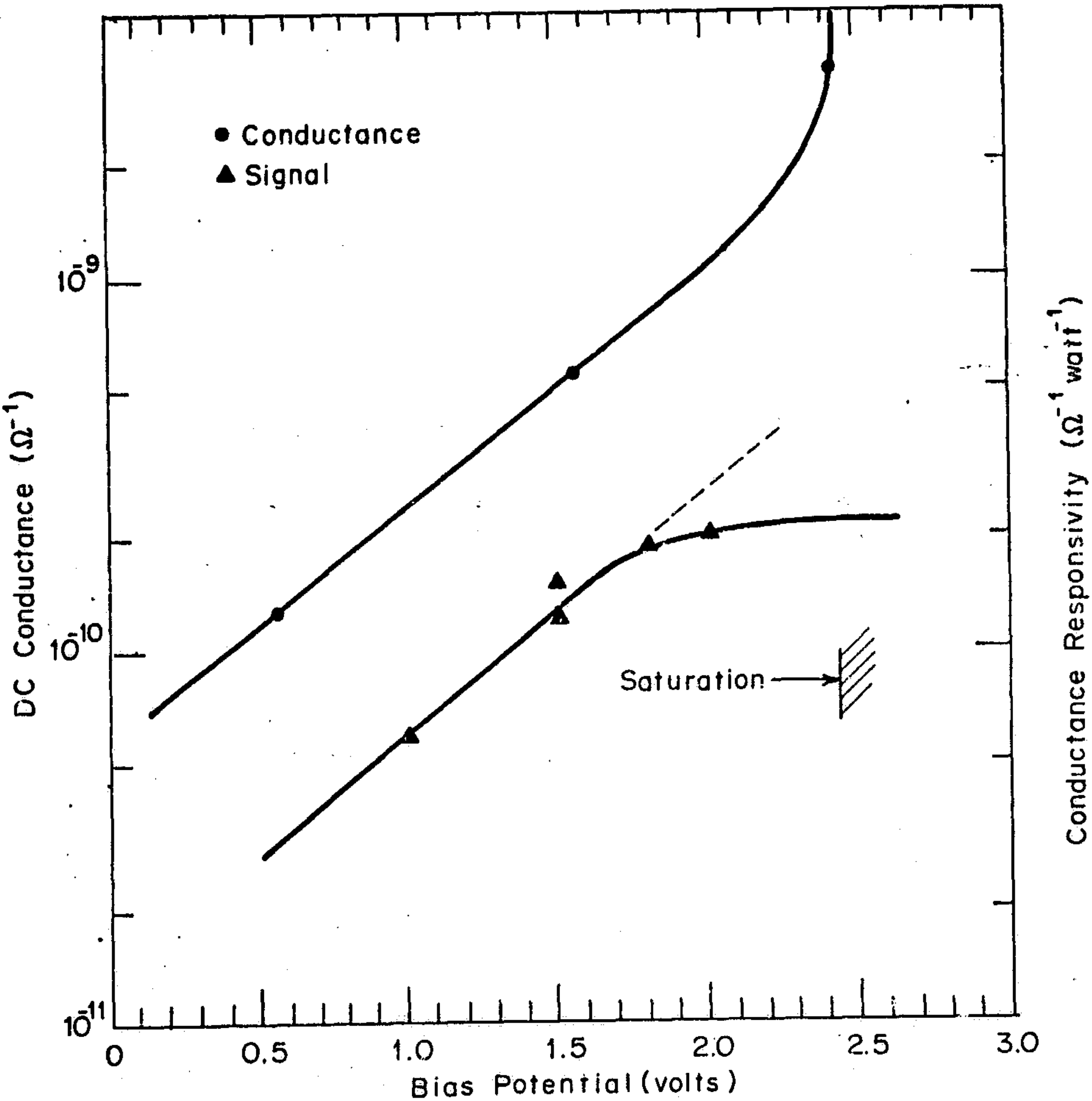
Conductance
Signal
10^{-9}
10^{-10}
10^{-11}
DC Conductance (Ω^{-1})
Conductance Responsivity (Ω^{-1} watt^{-1})
Saturation
0
0.5
1.0
1.5
2.0
2.5
3.0
Bias Potential (volts)

Figure 13

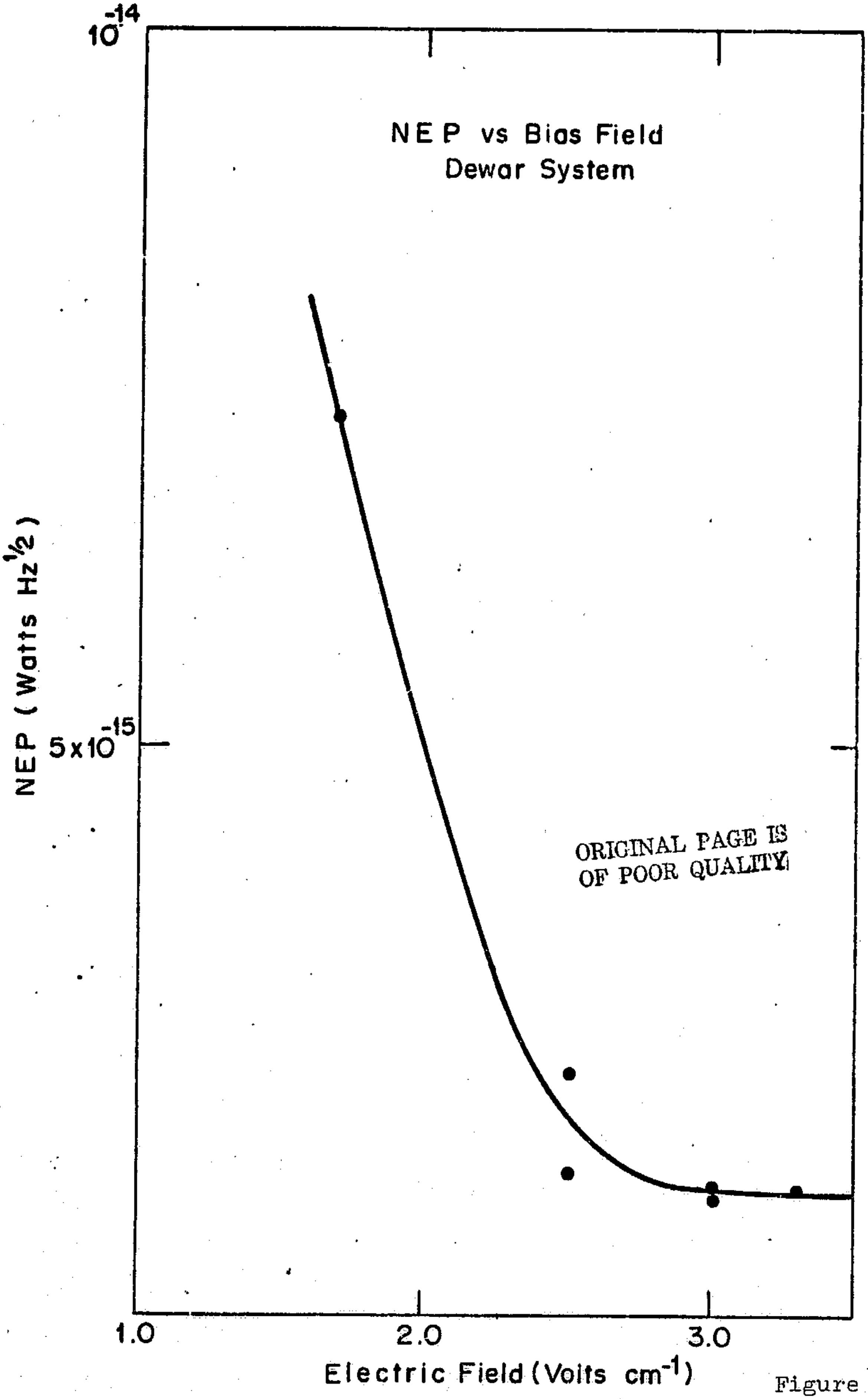
NEP vs Bias Field
Dewar System
10^{-14}
5×10^{-15}
NEP (Watts Hz$^{1/2}$)
1.0
2.0
3.0
Electric Field (Volts cm^{-1})

Figure 14